Improving the self-consistent predictions of texture development of polycrystals incorporating intragranular field fluctuations

Ricardo A. Lebensohn[1, a], Carlos N. Tomé[1,b] and Pedro Ponte Castañeda[2,c]

[1]Materials Science and Technology Division, Los Alamos National Laboratory, Los Alamos, NM, 87545, USA

[2]Département de Mécanique, Ecole Polytechnique, F 91 128 Palaiseau, France

[a]lebenso@lanl.gov, [b]tome@lanl.gov, [c]ponte@lms.polytechnique.fr

Keywords: self-consistent, second-order moments, field fluctuations, fcc, ice.

Abstract. In this contribution we present how to implement the calculation of average field fluctuations inside the grains of a thermoelastic aggregate in terms of the derivatives of the stress potential given by the standard linear self-consistent (SC) model, and how this statistical information can be used to generate second-order estimates for the mechanical behavior of non-linear viscoplastic polycrystals, by means of a rigorous non-linear homogenization procedure. To illustrate the differences between this second-order (SO) self-consistent approach and the classical first-order SC approximations, we compare them in terms of their predictions of the effective behavior of random fcc polycrystals as a function of their rate-sensitivity, and of the texture evolution in hcp ice polycrystals under uniaxial compression. In the latter case, the SO approximation is the only one able to predict a substantial accommodation of deformation by basal slip, even when the basal poles become strongly aligned with the compression direction and the basal slip systems became unfavorably oriented.

Introduction

The computation of the large strain mechanical behavior and the texture evolution of viscoplastic polycrystals using self-consistent models is nowadays a standard approach within the texture community. For this, several 'classical' SC approximations for non-linear materials are available (e.g. the *secant* [1], *tangent* [2,3] and *affine* [4] formulations), all of them based on linearization schemes at the local level that use information on field averages only, disregarding higher-order statistical information in the grains. However, the above assumption may be questionable for single-phase aggregates with low rate-sensitivity, or made of highly anisotropic grains, or for multiphase polycrystals. In all these cases, a strong directionality and large variations in local properties are to be expected. The non-dependence with higher-order statistical moments is particularly critical for the treatment of highly-contrasted materials, since such information is essential to capture—in an average sense—the effect of the strong deformation gradients that are likely to develop inside grains which are strongly non-linear, highly anisotropic, or adjacent to another phase. Consequently, when applied to materials with high contrast, the above *first-order* SC approaches can lead to large differences in the predicted behavior and microstructural evolution.

To overcome the above limitations, in this work we first present how to implement the calculation of *average field fluctuations* inside the grains of a thermoelastic aggregate in terms of the derivatives of the stress potential, which has to be determined by means of the standard SC model for linear polycrystals. In turn, the above statistical information can be used to generate more refined estimates for non-linear viscoplastic polycrystals by means of the variational *second-order* (SO) method of Ponte Castañeda [5]. Briefly, this rigorous non-linear homogenization procedure consists in expressing the effective potential of a non-linear viscoplastic polycrystal in terms of that of a linearly viscous polycrystal with properties that depend on the first- and second-order moments in the grains, and are determined from suitably-designed variational principles.

Finally, to illustrate the differences between the different SC approaches we compare the above first-order and second-order formulations in terms of their predictions of the effective behavior of

random fcc polycrystals, as a function of their rate-sensitivity, and of the texture evolution in hcp ice polycrystals under uniaxial compression.

Theory

In what follows, all the tensors are symmetric and represent incompressible magnitudes or properties. Therefore, they can be represented using the symmetric 'b-basis' components [6] where 2nd and 4th rank tensors are represented by 5-dim vectors and 5x5 matrices, respectively.

Self-consistent approximation for linear polycrystals. The effective behavior of a generalized linear 'thermoelastic' polycrystal is characterized by a stress potential $\widetilde{U}_T$ that may be written in the form [7]:

$$\widetilde{U}_T = \frac{1}{2}\widetilde{M} : (\Sigma \otimes \Sigma) + \widetilde{e} \cdot \Sigma + \frac{1}{2}\widetilde{g}\,, \tag{1}$$

such that $E = \widetilde{M} \cdot \Sigma + \widetilde{e}$, where Σ is the macroscopic stress, E should be interpreted as the macroscopic strain (in the case of an actual thermoelastic material) or strain-rate (for a linearly viscous material), and $\widetilde{M}$, $\widetilde{e}$ and $\widetilde{g}$ are the effective compliance, back-extrapolated strain (or strain-rate) and energy under zero applied stress, defined (in the case all grains have the same shape) by:

$$\widetilde{M} = \sum_r c^{(r)} M^{(r)} \cdot B^{(r)}\,,\quad \widetilde{e} = \sum_r c^{(r)} e^{(r)} \cdot B^{(r)}\,,\quad \widetilde{g} = \sum_r c^{(r)} e^{(r)} \cdot b^{(r)}\,, \tag{2}$$

where $c^{(r)}$ is the volume fraction associated with grain (r), $M^{(r)}$ and $e^{(r)}$ are the local compliance and back-extrapolated term of grain (r) (such that $\varepsilon = M^{(r)} \cdot \sigma + e^{(r)}$), and $B^{(r)}$ and $b^{(r)}$ are the stress concentrations tensors of grain (r), i.e.

$$\overline{\sigma}^{(r)} = B^{(r)} \cdot \Sigma + b^{(r)}\,, \tag{3}$$

where $\overline{\sigma}^{(r)}$ is the average stress of grain (r). Explicitly, the SC expressions of the tensors above are given by [8]:

$$B^{(r)} = \left(M^{(r)} + M^*\right)^{-1} \cdot \left(\widetilde{M} + M^*\right)\,,\quad b^{(r)} = \left(M^{(r)} + M^*\right)^{-1} \cdot \left(\widetilde{e} - e^{(r)}\right), \tag{4}$$

where the interaction tensor M^* is given by:

$$M^* = (I - S)^{-1} \cdot S \cdot \widetilde{M}\,, \tag{5}$$

with S being the Eshelby tensor, a function of $\widetilde{M}$ and the grain-shape.

Second-order moments of the stress field. The average second-order moment of the stress over grain (r) is given by [7]:

$$\overline{\sigma \otimes \sigma}^{(r)} = \frac{2}{c^{(r)}}\frac{\partial \widetilde{U}_T}{\partial M^{(r)}} = \frac{1}{c^{(r)}}\frac{\partial \widetilde{M}}{\partial M^{(r)}} : (\Sigma \otimes \Sigma) + \frac{2}{c^{(r)}}\frac{\partial \widetilde{e}}{\partial M^{(r)}} \cdot \Sigma + \frac{1}{c^{(r)}}\frac{\partial \widetilde{g}}{\partial M^{(r)}}\,. \tag{6}$$

Working with Eqs. $(2)_1$, (4) and (5), the first derivative in the right term can be obtained solving the following equation [9]:

$$\Omega_{ijkl}\frac{\partial\widetilde{M}_{kl}}{\partial M_{uv}^{(r)}}=\pi_{ij}^{(r,uv)}, \tag{7}$$

where Ω_{ijkl} and $\pi_{ij}^{(r,uv)}$ are given in the Appendix. Expression (7) is a linear system of 25 equations with 25 unknowns (i.e. the components of $\partial\widetilde{M}_{kl}/\partial M_{uv}^{(r)}$). This system can be solved for a given value of the Eshelby tensor derivatives $\partial S/\partial M_{uv}^{(r)}$. This a priori unknown derivative can be calculated in terms of the also unknown $\partial\widetilde{M}/\partial M_{uv}^{(r)}$ [9,10]. Therefore, the problem must be solved iteratively and should stop when the input and output values of $\partial S/\partial M_{uv}^{(r)}$ (and therefore those of $\partial\widetilde{M}/\partial M_{uv}^{(r)}$) coincide within certain tolerance.

In turn, the other two derivatives appearing in Eq. (6) can be calculated as [9]:

$$\frac{\partial\widetilde{e}_i}{\partial M_{uv}^{(r)}}=\theta_i^{(r,uv)}+\zeta_{ikl}\frac{\partial\widetilde{M}_{kl}}{\partial M_{uv}^{(r)}}\ ,\ \frac{\partial\widetilde{g}}{\partial M_{uv}^{(r)}}=\eta^{(r,uv)}+\vartheta_i\frac{\partial\widetilde{e}_i}{\partial M_{uv}^{(r)}}, \tag{8}$$

where ζ_{ikl}, ϑ_i, $\theta_i^{(r,uv)}$ and $\eta^{(r,uv)}$ are given in the Appendix.

Non-linear self-consistent extensions. Every non-linear extension of the SC formulation is based on a linearization of the actual non-linear local behavior. In the case of an aggregate of single crystal grains deforming by dislocation glide, the non-linear rate-sensitivity constitutive relation is approximated by:

$$\varepsilon=\gamma_o\sum_k\mu_{(k)}^{(r)}\left(\frac{\mu_{(k)}^{(r)}\cdot\sigma}{(\tau_o)_{(k)}}\right)^n\cong M^{(r)}\cdot\sigma+e^{(r)}, \tag{9}$$

where $(\tau_o)_{(k)}$ and $\mu_{(k)}^{(r)}$ are the critical stress and the Schmid tensor associated with slip system (k), γ_o is a normalization factor, and n is the rate-sensitivity exponent. If $M^{(r)}$ and $e^{(r)}$ are chosen to be certain functions of the average stress $\overline{\sigma}^{(r)}$ in grain (r), the corresponding non-linear SC extension is known as a first-order approximation. Otherwise, if both $\overline{\sigma}^{(r)}$ and $\overline{\sigma\otimes\sigma}^{(r)}$ are involved in the determination of $M^{(r)}$ and $e^{(r)}$, the resulting SC approach becomes a second-order approximation.

First-order SC approximations. The three classical first-order approximations correspond to the following assumptions:

$$M_{sec}^{(r)}=\gamma_o\sum_k\frac{\mu_{(k)}^{(r)}\otimes\mu_{(k)}^{(r)}}{(\tau_o)_{(k)}}\left(\frac{\mu_{(k)}^{(r)}\cdot\overline{\sigma}^{(r)}}{(\tau_o)_{(k)}}\right)^{n-1},\ e_{sec}^{(r)}=0 \qquad (\textit{secant}) \tag{10}$$

$$M_{aff}^{(r)} = n\gamma_o \sum_k \frac{\mu_{(k)}^{(r)} \otimes \mu_{(k)}^{(r)}}{(\tau_o)_{(k)}} \left(\frac{\mu_{(k)}^{(r)} \cdot \overline{\sigma}^{(r)}}{(\tau_o)_{(k)}} \right)^{n-1}, \quad e_{aff}^{(r)} = \left(M_{sec}^{(r)} - M_{aff}^{(r)} \right) : \overline{\sigma}^{(r)} \qquad \textit{(affine)} \tag{11}$$

In the case of the *tangent* approximation, $M_{tg}^{(r)} = M_{aff}^{(r)}$ and $e_{tg}^{(r)} = e_{aff}^{(r)}$. However, instead of using expressions (11) in the self-consistent equations (2), use is made of the secant scheme to get $\widetilde{M}_{sec}$, which, in combination with the tangent-secant relation $\widetilde{M}_{tg} = n\widetilde{M}_{sec}$ [1], allows calculating the interaction tensor as:

$$M_{tg}^{*} = (I - S)^{-1} \cdot S \cdot \widetilde{M}_{tg} = n(I - S)^{-1} \cdot S \cdot \widetilde{M}_{sec}. \tag{12}$$

This algorithmic difference makes the tangent formulation tend to the lower-bound at low rate-sensitivities.

Second-order procedure. Once the average second-order moments of the stress field over each grain are obtained by means of the calculation of the derivatives appearing in Eq. (6), the implementation of the SO procedure follows the work of Liu and Ponte Castañeda [7]. The covariance tensor of stress fluctuations is given by:

$$C_{\sigma}^{(r)} = \overline{\sigma \otimes \sigma}^{(r)} - \overline{\sigma}^{(r)} \otimes \overline{\sigma}^{(r)}. \tag{13}$$

The average and the average fluctuation of resolved shear stress on slip system (k) of grain (r) is given by:

$$\overline{\tau}_{(k)}^{(r)} = \mu_{(k)}^{(r)} \cdot \overline{\sigma}^{(r)}, \quad \hat{\tau}_{(k)}^{(r)} = \overline{\tau}_{(k)}^{(r)} \pm \left(\mu_{(k)}^{(r)} \cdot C_{\sigma}^{(r)} \cdot \mu_{(k)}^{(r)} \right)^{1/2}, \tag{14}$$

where the positive (negative) branch should be selected if $\overline{\tau}_{(k)}^{(r)}$ is positive (negative). The slip potential of slip system (k) in every grain is defined as:

$$\phi_{(k)}(\tau) = \frac{(\tau_o)_{(k)}}{n+1} \left(\frac{|\tau|}{(\tau_o)_{(k)}} \right)^{n+1}. \tag{15}$$

Two scalar magnitudes associated with each slip system (k) of each grain (r) are defined by:

$$\alpha_{(k)}^{(r)} = \frac{\phi'^{(r)}_{(k)}\left(\hat{\tau}_{(k)}^{(r)}\right) - \phi'^{(r)}_{(k)}\left(\overline{\tau}_{(k)}^{(r)}\right)}{\hat{\tau}_{(k)}^{(r)} - \overline{\tau}_{(k)}^{(r)}}, \quad e_{(k)}^{(r)} = \phi'^{(r)}_{(k)}\left(\overline{\tau}_{(k)}^{(r)}\right) - \alpha_{(k)}^{(r)} \overline{\tau}_{(k)}^{(r)}. \tag{16}$$

where $\phi'_{(k)}(\tau) = d\phi_{(k)} / d\tau(\tau)$. The linearized local behavior associated with grain (r) is then given by $\varepsilon = M_{so}^{(r)} \cdot \sigma + e_{so}^{(r)}$, where:

$$M_{so}^{(r)} = \sum_k \alpha_{(k)}^{(r)} \left(\mu_{(k)}^{(r)} \otimes \mu_{(k)}^{(r)} \right), \quad e_{so}^{(r)} = \sum_k e_{(k)}^{(r)} \mu_{(k)}^{(r)}. \tag{17}$$

The SO procedure requires iterating over $M_{so}^{(r)}$ and $e_{so}^{(r)}$ to derive improved estimations of a linear comparison polycrystal. Each of these polycrystals has associated different first- and second-order moments of the stress field in the grains. These statistical moments can be used to obtain new values of $\alpha_{(k)}^{(r)}$ and $e_{(k)}^{(r)}$, which in turn define a new linear comparison polycrystal, etc. This convergence procedure is terminated when the input and output values of $\alpha_{(k)}^{(r)}$ and $e_{(k)}^{(r)}$ coincide within a certain tolerance.

Results

Effective behavior of random fcc polycrystals. The prediction of the effective properties of a random fcc polycrystal as the rate-sensitivity of the material decreases is a classical benchmark for the different non-linear SC extensions. Figure 1 shows a comparison between Taylor Factor (TF) vs. rate-sensitivity (1/n) curves, for a random fcc polycrystal under uniaxial tension. The TF was calculated as Σ_{eq}/τ_o, where τ_o is the threshold stress of the (111)<110> slip systems, and Σ_{eq} is the macroscopic equivalent stress corresponding to an unitary applied equivalent strain-rate $E_{eq}=1$. The different curves correspond to the Taylor model, the different first-order SC approximations, and the second-order procedure. It can be observed that:

a) The TF curve predicted with Taylor approach is the highest, consistent with the upper bound status of this model.

b) All SC estimates coincide for n=1, i.e. the linear SC case.

c) For high and moderate rate-sensitivities, the SO procedure gives the lowest TF among the SC approaches. This is the reflection of an effective softer behavior at grain level that occurs when field fluctuations are considered for the determination of the linearized behavior of the grains.

d) In the rate-insensitive limit, while the secant and the tangent models tend respectively to the upper bound (Taylor) and the lower bound (i.e. TF=2.2 for $1/n \to 0$), the affine and SO approximations give intermediate results.

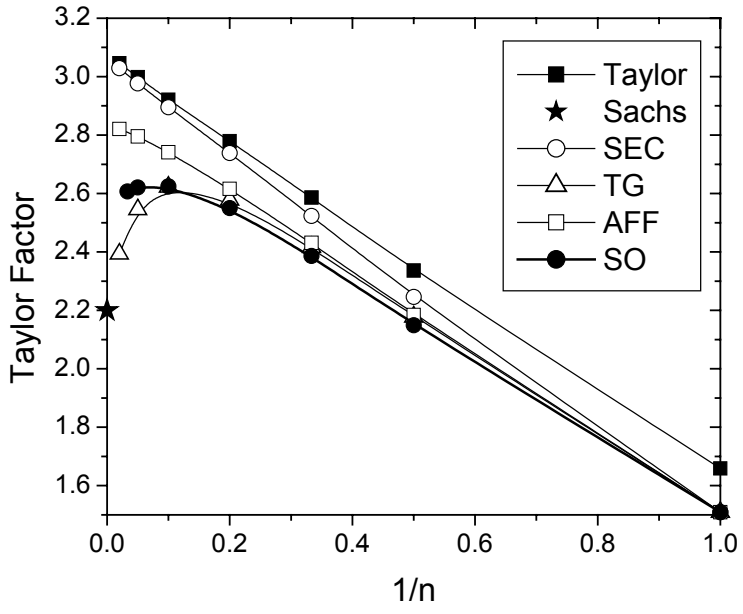

Figure 1: Taylor Factor vs. rate-sensitivity, for a random fcc polycrystal under unixial tension, as predicted with the Taylor model, several first-order SC approximations, and the second-order procedure.

Texture evolution in ice polycrystals. Due to the very large plastic anisotropy of hcp ice (i.e. while almost all the deformation in the single crystals is carried by basal dislocations, basal slip provides only two independent slip systems), the prediction of texture development of polycrystalline ice is a challenging problem serving to discriminate among the various SC approaches. Moreover, a better understanding of the deformation mechanisms and the microstructural evolution of ice deforming in compression is relevant in glaciology, since compression (together with shear) is one of the main deformation modes of glacier ice. In what follows, we will use the basal texture factor along the axial direction (defined as the weighted average of the projections of the c-axis along that direction) to characterize the evolving texture of ice in compression.

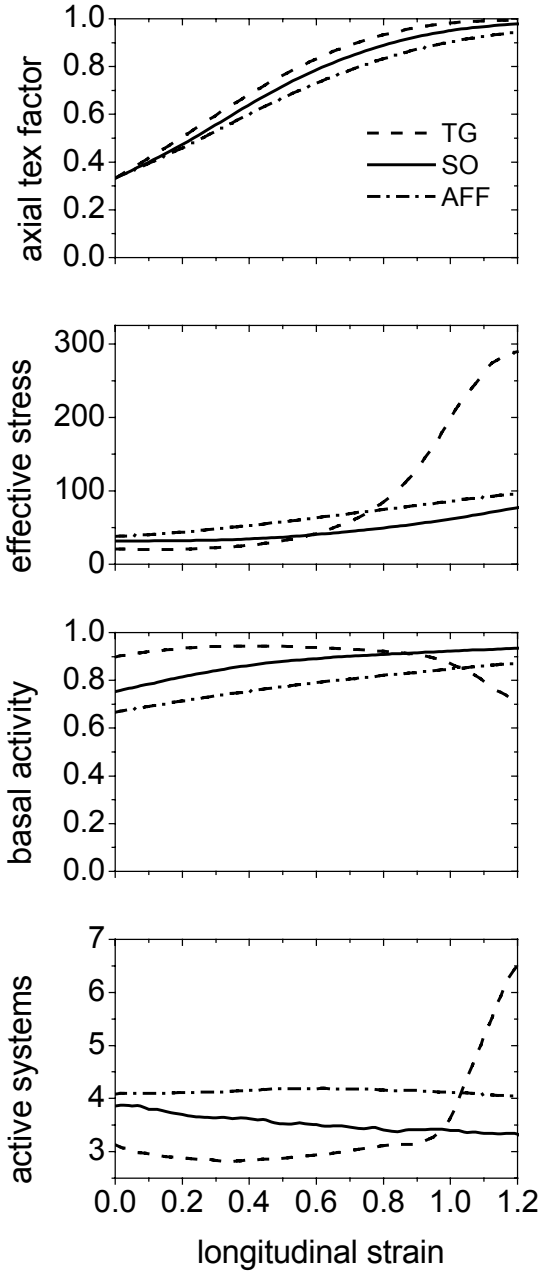

Figure 2: Basal texture factor along the compression direction, effective stress, relative basal activity, and the average number of active slip systems per grain. Case of compression of an initially random ice polycrystal with $\tau_{pr}=20\times\tau_{bas}$ and $\tau_{pyr}=200\times\tau_{bas}$ [11], as predicted with the tangent, affine and second-order SC approaches.

On the one hand, the 'stiff' Taylor and SC secant models are not suitable to simulate plastic deformation of polycrystalline ice because the strong constraints that these models impose upon strain are incompatible with the shortage of independent slip systems in ice. On the other hand, the compression textures of ice typically exhibit a strong basal pole maximum along the axial direction [11]. The formation of this maximum is related with the crystallographic plastic rotations associated with basal slip. However, as the basal poles become aligned with the axial direction, the basal slip systems become unfavorably oriented to accommodate deformation. Therefore, at large strains, even a 'soft' model like the tangent SC fails in reproducing the observed texture, with only basal slip [11]. Up to now, the oversimplified Sachs model (which completely disregards strain compatibility) has been the only approach able to give a reasonable effective behavior with predominant basal slip at large strains, when the basal texture along the compressive direction becomes very strong.

For comparison between the different SC approaches, Fig. 2 shows the compression texture evolution (in terms of the basal texture factor along the axial direction), the effective stress, the relative basal activity, and the average number of active slip systems per grain, for the case of an initially random ice polycrystal, under the assumption of $\tau_{pr} = 20 \times \tau_{bas}$ and $\tau_{pyr}=200\times\tau_{bas}$, where τ_{bas}, τ_{pr} and τ_{pyr} are the critical stresses of the $(0001)\langle 1120\rangle$ *basal*, $\{1010\}\langle 1120\rangle$ *prismatic* and $\{1122\}\langle 1123\rangle$ *pyramidal* slip modes, respectively, as reported in [11].

As expected, all models predict an increase of the basal texture factor along the axial direction, and a progressive geometric hardening. The tangent and the affine SC models predict the fastest and the slowest alignment of basal poles along the compression direction. This is consistent with the initial highest basal activity predicted by the tangent model, followed by the ones obtained with the SO and the affine formulations. However, at around 0.8 strain, the tangent results show a sudden drop in the basal activity, together with an increase in the effective stress (not attributable to geometric hardening only) and in the number of active deformation systems. All this indicates that, at large compressive deformation, the strain accommodation starts requiring the activation of the 200 times harder pyramidal systems. In other words, under the tangent SC approach, the basal slip by itself is not enough to accommodate the compressive deformation when the basal poles become strongly aligned with the compression direction.

The SO results are superior to the affine results, since the deformation takes place at higher basal activities, and also to the tangent results, since the SO model does not require the activation of the hard pyramidal mode, even after the texture factor reaches the value at which the tangent model predictions start to deteriorate.

This superior performance of the second-order SC approximation can be explained in terms of its intrinsic adaptability to microstructural changes. Figure 3 shows the evolution (as predicted with the SO formulation) of the normalized standard deviation (SD) of the equivalent stress and strain rate over the whole polycrystal, defined as:

$$\mathrm{SD}\left(\sigma_{eq}\right)=\sqrt{\overline{\overline{\Sigma}}_{eq}^{2}-\Sigma_{eq}^{2}}\,/\,\Sigma_{eq}\,,\ \mathrm{SD}\left(\varepsilon_{eq}\right)=\sqrt{\overline{\overline{E}}_{eq}^{2}-E_{eq}^{2}}\,/\,E_{eq}\,, \tag{18}$$

where:

$$\overline{\overline{\Sigma}}_{eq}^{2}=\sum_{r} c^{(r)}\left(\overline{\overline{\sigma}}_{eq}^{(r)}\right)^{2}\ ,\ \overline{\overline{E}}_{eq}^{2}=\sum_{r} c^{(r)}\left(\overline{\overline{\varepsilon}}_{eq}^{(r)}\right)^{2}\,, \tag{19}$$

where second-order moments in grain (r) are given by:

$$\overline{\overline{\sigma}}_{eq}^{(r)} = \left(\frac{3}{2} \mathbf{I} : \overline{\sigma \otimes \sigma}^{(r)} \right)^{1/2} , \quad \overline{\overline{\varepsilon}}_{eq}^{(r)} = \left(\frac{2}{3} \mathbf{I} : \overline{\varepsilon \otimes \varepsilon}^{(r)} \right)^{1/2} . \tag{20}$$

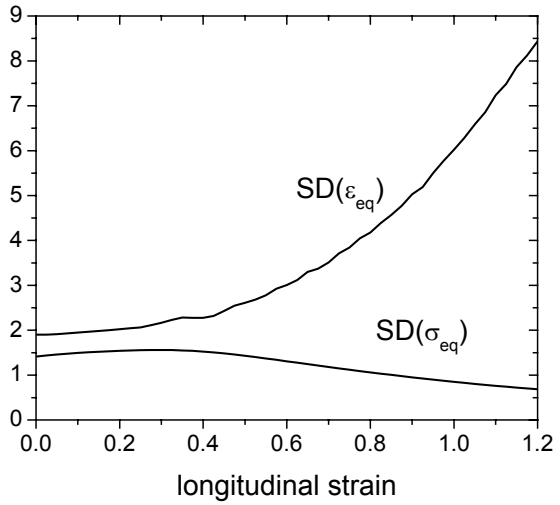

Figure 3: Evolution of the normalized standard deviations of the equivalent stress and strain rate, as predicted with the SO formulation, for the case of compression of ice.

Note that the above magnitudes are indicators not only of intergranular, but also of intragranular heterogeneity. Evidently, as the basal texture concentrates along the axial direction, the stress becomes more uniform and the strain rate becomes more heterogeneous. This trend towards a uniform stress state obviously indicates a trend towards the Sachs hypothesis. Therefore, given that the fluctuation information is contained in the SO formulation, the SO results should come closer to Sachs as deformation proceeds, allowing a substantial accommodation of deformation by basal slip at those large strains.

Summary

A methodology for the calculation of second-order moments of the mechanical fields inside the grains of a polycrystal, within the framework of SC models, has been given. Using the stress second-order moments inside the grains, the second-order SC procedure was implemented, and its results where compared with other SC approximations for the cases of the effective properties of random fcc aggregates with different rate sensitivities, and for the texture evolution of ice polycrystals under compression. In the latter case, the SO model predicts a substantial accommodation of deformation by basal slip, even when the basal poles became strongly aligned with the compression direction and the basal slip systems became unfavorably oriented.

References

[1] J.W. Hutchinson: Proc. R. Soc. London A Vol. 348 (1976), p. 101.

[2] A. Molinari, G.R. Canova and S. Ahzi: Acta metall. Vol. 35 (1987), p. 2983.

[3] R.A. Lebensohn and C.N. Tomé: Acta metall. mater. Vol. 41(1993), p. 2611.

[4] R. Masson, M. Bornert, P. Suquet and A. Zaoui: J. Mech. Phys. Solids Vol. 48 (2000), p. 1203.

[5] P. Ponte Castañeda: J. Mech. Phys. Solids Vol 50 (2002), p. 737.

[6] R.A. Lebensohn, P.A. Turner, J.W. Signorelli, G.R. Canova and C.N. Tomé: Modelling Simul. Mater. Sci. Eng. Vol. 6 (1998), p. 447.

[7] Y. Liu and P. Ponte Castañeda: J. Mech. Phys. Solids Vol. 52 (2004), p. 467.

[8] R.A. Lebensohn, C.N. Tomé and P.J. Maudlin: J. Mech. Phys. Solids Vol. 52 (2004), p. 349.

[9] R.A. Lebensohn and C.N. Tomé: Los Alamos National Laboratory Report, to be published.

[10] J.W. Signorelli, R. Logé, Y. Chastel and R.A. Lebensohn: Modelling Simul. Mater. Sci. Eng. Vol. 8 (2000), p. 1983.

[11] O. Castelnau, P. Duval, R. A. Lebensohn and G.R. Canova: J Geophys. Res B Vol 101 (1996), p. 13851

Appendix

Defining the following auxiliary magnitudes:

$$\chi^{(r)} = \left(M^{(r)} + M^{*}\right)^{-1} \ , \ \beta^{(r)} = M^{(r)} \cdot \left(M^{(r)} + M^{*}\right)^{-1} \ , \ F = (I - S)^{-1} \cdot S \tag{A1}$$

$$\Phi^{(r)} = (I - S)^{-1} \cdot \frac{\partial S}{\partial M^{(r)}_{uv}} \cdot \left[F \cdot \tilde{M} + \tilde{M}\right] , \ \alpha^{(r)}_{ijkl} = F_{ik}\left(I - B^{(r)}\right)_{lj} + \delta_{ik}\delta_{jl} \tag{A2}$$

$$\lambda^{(r)} = \sum_{s} c^{(s)}\beta^{(s)} \cdot \Phi^{(r)} \cdot \left(I - B^{(s)}\right) , \ \Omega' = \sum_{r} c^{(r)}\beta^{(r)} \cdot \alpha^{(r)} \tag{A3}$$

$$\kappa = \sum_{r} c^{(r)} e^{(r)} \cdot \chi^{(r)} \cdot \Phi^{(r)} \cdot \left(I - B^{(r)}\right) \tag{A4}$$

$$\nu = -\sum_{r} c^{(r)} e^{(r)} \cdot \chi^{(r)} \cdot \left(\Phi^{(r)} + F \cdot \frac{\partial \tilde{M}}{\partial M^{(r)}_{uv}} \right) \cdot \chi^{(r)} \cdot \left(\tilde{e} \ - e^{(r)}\right) , \tag{A5}$$

the coefficients in Eqs.(7) and (8) are [9]:

$$\Omega_{ijkl} = \delta_{ik}\delta_{jl} - \Omega'_{ijkl} \ , \ \pi^{(r,uv)}_{ij} = c^{(r)}\left(\delta_{iu} - \beta^{(r)}_{iu}\right)B^{(r)}_{vj} + \lambda^{(r)}_{ij} \tag{A6}$$

$$\zeta_{ijk} = \sum_{r} c^{(r)} e^{(r)}_{m} \chi^{(r)}_{ml} \alpha^{(r)}_{lijk} \ , \ \theta^{(r,uv)}_{i} = -c^{(r)} e^{(r)}_{m} \chi^{(r)}_{mu} B^{(r)}_{vi} + \kappa_i \tag{A7}$$

$$\vartheta_i = \sum_{s} c^{(r)} e^{(r)}_{m} \chi^{(r)}_{mi} \ , \ \eta^{(r,uv)} = -c^{(r)} e^{(r)}_{m} \chi^{(r)}_{mu} \chi^{(r)}_{vl} \left(\tilde{e}_l - e^{(r)}_{l}\right) + \nu \, . \tag{A8}$$